Geomorphology 105 (2009) 366–373

Contents lists available at ScienceDirect

Geomorphology

journal homepage: www.elsevier.com/locate/geomorph

An integrated model for predicting rainfall-induced landslides

Kang-Tsung Chang [a,*], Shou-Hao Chiang [b]

[a] Kainan University, Taoyuan County 33857, Taiwan
[b] Department of Geography, National Taiwan University, Taipei 106, Taiwan

ARTICLE INFO

Article history:
Received 8 August 2008
Received in revised form 17 October 2008
Accepted 21 October 2008
Available online 29 October 2008

Keywords:
Integrated model
Critical rainfall model
Logit model
Radar rainfall estimate
Typhoon

ABSTRACT

This study proposes a novel method that combines a deterministic slope stability model and a statistical model for predicting rainfall-induced landslides. The method first uses the deterministic model to derive the rainfall rate critical to induce slope failure for each land unit. Then it calculates the difference between the critical rainfall threshold and estimated rainfall intensity. Using the difference and estimated rainfall duration as explanatory variables, the method derives a logit (integrated) model to compute landslide occurrence probabilities. To demonstrate the effectiveness of this method, the study used radar rainfall estimates and landslides associated with a typhoon (tropical cyclone) to develop the integrated model and the same types of data associated with another typhoon to validate the model. The model had a modified success rate of 84.0% for predicting landslides and stable areas, and model validation yielded a modified success rate of 87.4%. Both rates were better than those from the critical rainfall model. The main advantage of the integrated model lies in its use of rainfall variables that are not included in calculating the critical rainfall. Also, as a probabilistic model, the integrated model is better suited for decision-making in watershed management. This study has advanced the method for predicting rainfall-triggered landslides.

1. Introduction

Landslide is a widespread hazard in mountainous regions around the world (Aleotti and Chowdhury, 1999; Guzzetti et al., 1999; Dai et al., 2002). Landslides cause not only considerable financial losses but also major ecological and environmental problems such as increased soil erosion rate and downstream sediment load (Hovius et al., 1997; Claessens et al., 2007). It is well known that many landslides, especially shallow ones, are triggered by rainfall; therefore, how to improve landslide modeling and prediction by using rainfall data has become an important research topic (Chang et al., 2008).

The literature has so far suggested three major avenues of predicting areas prone to rainfall-induced slope failures. First, researchers have plotted historical data to find rainfall thresholds likely to trigger landslides. The two early works of Campbell (1975) and Caine (1980) were followed by numerous studies from different parts of the world (Cannon and Ellen, 1985; Au, 1993; Larsen and Simon, 1993; Finlay et al., 1997; Crozier, 1999; Glade et al., 2000; Aleotti, 2004; Guzzetti et al., 2004; Ibsen and Casagli, 2004; Baum et al., 2005; Chen et al., 2005, 2007; Godt et al., 2006). However, without involving site-specific data that separate landslides from non-landslide areas, rainfall threshold studies cannot shed light on the interaction of rainfall and local topography in causing landslides (Chang et al., 2008).

Second, researchers have combined steady-state hydrologic concepts and the infinite slope stability model to estimate the critical rainfall (the minimum steady-state rainfall) for slope failure (Montgomery and Dietrich, 1994; Wu and Sidle, 1995; Pack et al., 1998; Borga et al., 2002; Casadei et al., 2003). Conceptually, the critical rainfall model is applicable to different geographic areas (Montgomery et al., 2002). However, the model typically requires local topographic and soil parameters that are difficult to gather, especially over large and complex areas (Gorsevski et al., 2006; Carrara et al., 2008). In many cases, estimated data or surrogate variables are used for model building, causing uncertainty of varying degrees in the model result. Also, being deterministic, the critical rainfall model does not offer confidence measures, thus limiting its application in decision-making for watershed management.

Third, researchers have used statistical techniques to evaluate the spatial distribution of landslides with site-specific topographic attributes, lithology, land-cover, and land-use (Dai and Lee, 2003; Ohlmacher and Davis, 2003; Ayalew and Yamagishi, 2005; Can et al., 2005; Yesilnacar and Topal, 2005; Chang et al., 2007). Primarily due to the lack of reliable and high-resolution rainfall fields, few statistical models have included rainfall variables as explanatory variables. An exception is our previous study in which two rainfall variables, maximum 3-h rainfall intensity and total rainfall duration, were used as explanatory variables (Chang et al., 2008). Because statistical models treat landsliding as a 'black box', they are unable to contribute to a better understanding of the physical processes of landsliding.

This paper proposes a novel method that combines a deterministic slope stability model and a statistical (logit) model, and incorporates

* Corresponding author. Tel.: +886 33412500x1021; fax: +886 33413252.
E-mail address: chang@uidaho.edu (K.-T. Chang).

0169-555X/$ – see front matter © 2008 Elsevier B.V. All rights reserved.
doi:10.1016/j.geomorph.2008.10.012

rainfall data directly into landslide modeling and prediction. This method first derives for each land unit (cell) the critical rainfall, a rainfall rate calculated from local topographic and soil attributes. The method then measures the rainfall intensity difference (RID): the amount of rainfall intensity that is above (or below) the critical rainfall, estimated from radar imagery. It is assumed that slope failures will more likely occur in areas, where RID is large and positive (i.e., estimated rainfall intensity>critical rainfall threshold). Then a logit model is developed using RID and rainfall duration as explanatory variables. It is assumed that rainfall duration, a variable not considered in the critical rainfall model, can help predict landslide occurrence. The logit model is integrated because it combines a deterministic model and a statistical model. More importantly, it is integrated because it pulls together local topographic and soil properties and rainfall variables in estimating the probability of landslide occurrence. To show how the method works, this study uses radar rainfall estimates and landslides associated with a typhoon (tropical cyclone) to develop the integrated model and the same types of data from another typhoon to validate the model. The study then compares the performance of the integrated model with that of the critical rainfall model, before discussing the potential application of the integrated model.

2. Regional setting

The study area is the 120 km^2 Baichi watershed in northern Taiwan (Fig. 1). It is located on the west side of the Central Mountain Range in the Eo-Oligocene argillite-slate belt. This watershed regularly experiences landslides triggered by typhoons because Taiwan has an average of four typhoons per year (Wu and Kuo, 1999). Three major lithological formations in the Baichi watershed are the Aoti formation with shale and argillite, the Tatungshan formation with slate and phyllite, and the Kanko formation with shale, slate, and argillite. Bedrocks are heavily fractured by joints from folding and faulting. Soil depths range from 0.8 to 1.3 m. Shallow soils are dominated by frequent erosion on steep slopes while soils with a thicker layer occupy lower slopes and valleys.

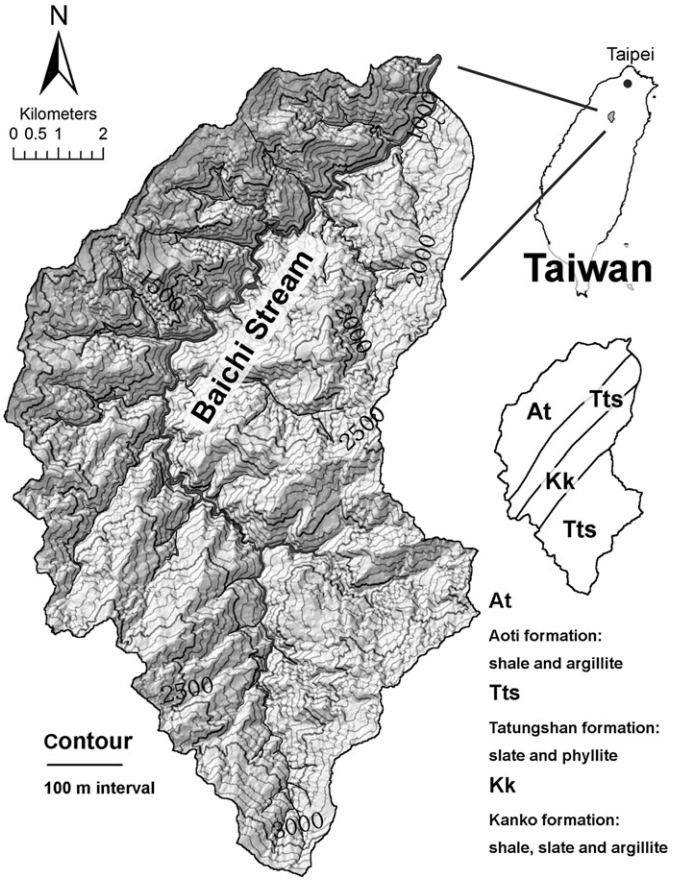

Fig. 1. Location and the lithological settings of the Baichi watershed.

Elevations in the watershed range from 830 m a.s.l. in the northwest to 3320 m in the southeast, with generally rugged topography. About 90% of the study area is forested: natural needle- and broad-leaf mix accounts for 33%, natural broad-leaf forest 33%, natural needle-leaf forest 15%, and plantation forest 10%. Areas in the remaining 10% are cultivated fields and built-up areas located in lower elevations of the northern part of the watershed. The climate is influenced by typhoons in summer and the northeast monsoon in winter. The mean monthly temperature is 27.5 °C in July and 14.2 °C in January, with the mean annual temperature of 21 °C. The annual precipitation averages 2370 mm, 46% of which occurs between June and September during the typhoon season. As the upstream area of the Shihmen Reservoir, the largest multi-purpose reservoir in northern Taiwan, the Baichi watershed is frequently monitored and has more data available than other mountainous watersheds.

3. Materials and methods

3.1. Typhoons Aere and Haitang

Two major typhoons in recent years, Aere and Haitang, were selected for model development and validation, respectively. On August 23–25, 2004, Typhoon Aere crossed the northern tip of the island in an east–west direction before turning southwestward. During its peak on August 24, Typhoon Aere had a 200-km storm radius and a low pressure reading of 955 hPa, packing winds of 140 km h^{-1} and gusts to 175 km h^{-1}. Typhoon Haitang rotated off the east coast of Taiwan for more than 6 h before making landfall on July 18, 2005. The storm then moved west–northwesterly across the center of the island and entered the Taiwan Strait on July 19. During its peak intensity, Typhoon Haitang had a low pressure reading of 915 hPa, packing winds of 195 km h^{-1} and gusts to 260 km h^{-1}.

Based on pressure reading and wind velocity, Haitang was a stronger typhoon than Aere. But Aere was a far more severe and destructive rainfall event than Haitang. Baichi, a gauge station located in the center of the watershed, recorded 1607 mm of total rainfall and 52.6 mm h^{-1} of maximum 24-h rainfall intensity during Typhoon Aere and 396 mm and 12.8 mm h^{-1} during Typhoon Haitang. As a rainfall event, Aere was four times larger than Haitang. Haitang, however, had longer rainfall duration (69 h) than Aere (57 h).

3.2. Landslide data

New landslides triggered by typhoons Aere and Haitang were interpreted and mapped by comparing ortho-rectified aerial photographs taken before and after the typhoon (Table 1). These color orthophotographs were compiled by the Aerial Survey Office of Taiwan's Forestry Bureau from the stereo pairs of 1:5000 aerial photographs. They have a pixel size of 0.35 m and an estimated horizontal accuracy of 0.5 m. There were 421 landslides triggered by Typhoon Aere and 259 by Typhoon Haitang. Most observed slope failures were shallow landslides on soil mantled slopes with depth less than 2 m. Table 1 summarizes the descriptive statistics of these landslides, and Fig. 2 shows their spatial distributions. For data analysis, landslide polygons were rasterized using a cell resolution of 10 m.

3.3. Radar rainfall estimates

The Central Weather Bureau (CWB) of Taiwan maintains the QPESUMS (quantitative precipitation estimation and segregation

Table 1
Image data sources and descriptive statistics of landslides triggered by Typhoon Aere (n=421) and Typhoon Haitang (n=259)

Typhoon event	Dates of aerial photographs	Landslide statistics (area unit: ha)				
		Sum	Max	Min	Mean	SD
Aere (Aug. 23–25, 2004)	Aug. 6, 2004 / Sep. 2, 2004	267.46	45.93	<0.10	0.63	2.45
Haitang (July 16–19, 2005)	Jan. 17, 2005 / May 11, 2006	62.91	2.97	<0.10	0.24	0.34

using multiple sensors), a system that collects data from a network of four Doppler radars for estimating rainfall field and depth (Chen et al., 2007). It records base (lowest elevations without blockages) reflectivity with a spatial resolution of 0.0125° (~1.25 km) in both longitude and latitude and a temporal resolution of 10 min.

The CWB provided radar reflectivity data for August 23–25, 2004, corresponding to the event of Typhoon Aere, for the study area. First, we summed the 10-minute radar reflectivity data by hour and divided the sum by six for the hourly average. Then we projected the radar data onto a 12-by-20 grid with a spatial resolution of 1 km and converted the hourly average reflectivity data into hourly rainfall data. The conversion developed by the CWB uses a power relationship to transform radar reflectivity into rainfall rate, followed by calibration using an inverse distance weighted method and rain gauge measurements (Chang et al., 2008). The calibration is needed to correct radar rainfall bias (Krajewski and Smith, 2002; Creutin and Borga, 2003). For radar rainfall calibration in this study, we collected ground rainfall measurements from six automatic rain gauges: one (Baichi) is located within the study area and the other five are within 1 to 10 km from the watershed boundary. Finally, we derived maximum 24-h rainfall intensity and rainfall duration for each 1-km cell from the hourly rainfall data. The same procedure was followed to obtain rainfall estimates associated with Typhoon Haitang for model validation.

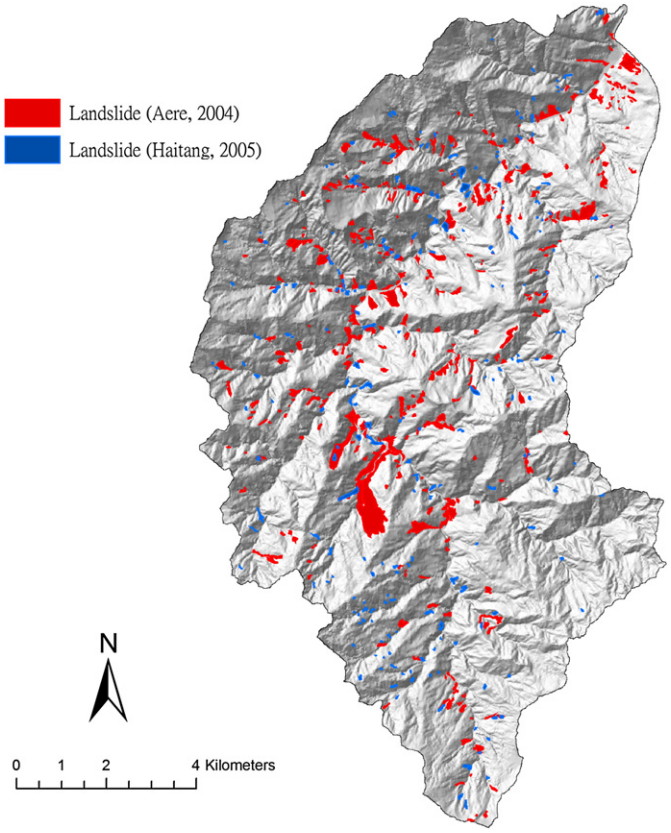

Fig. 2. Landslides triggered by typhoons Aere and Haitang.

3.4. Critical rainfall model and input parameters

The critical rainfall model is based on the steady-state assumption, implying that the specific upslope area can be a surrogate measure of the subsurface flow at any point in the landscape (Montgomery and Dietrich, 1994). The critical rainfall, Q_{cr}[mm day^{-1}], can be computed by:

$$Q_{cr} = T\sin\theta\left(\frac{b}{a}\right)\left(\frac{\rho_s}{\rho_w}\right)\left[1-\frac{(\sin\theta - C)}{(\cos\theta\tan\phi)}\right] \quad (1)$$

where T is saturated soil transmissivity [L^2 T^{-1}]; θ the local slope angle [°]; a the upslope contributing drainage area [L^2]; b the unit contour length (the grid resolution) [L]; ρ_s wet soil bulk density [g cm^{-1}]; ρ_w the density of water [g cm^{-3}]; ϕ the effective angle of internal friction of soil [°]; and C the combined cohesion term [−], made dimensionless relative to perpendicular soil thickness D[L] and defined as:

$$C = \frac{C_r + C_s}{D\rho_s g} \quad (2)$$

where C_r is root cohesion [N m^{-2}], C_s soil cohesion [N m^{-2}], and g the gravitational acceleration constant (9.81 m s^{-1}).

Critical rainfall values calculated from Eq. (1) are bounded by unconditionally stable and unstable areas. Unconditionally stable areas are areas predicted to be stable even when saturated and satisfy:

$$\tan\theta \le \left(\frac{C}{\cos\theta}\right) + \left(1-\frac{\rho_w}{\rho_s}\right)\tan\phi \quad (3)$$

Unconditionally unstable areas are areas predicted to be unstable even when dry and satisfy:

$$\tan\theta > \tan\phi + \left(\frac{C}{\cos\theta}\right) \quad (4)$$

To compute the critical rainfall, a soil thickness of 1 m based on our field observations was used. Three soil physical characteristics, ρ_s, T, and C_s, were measured from 14 data points representing the three lithological formation units in the study area (Table 2). The NDVI (normalized difference vegetation index) values retrieved from the 8-m FORMOSAT-2 satellite images taken on July 8, 2004 were used to estimate the spatial variation of C_r. For each cell, we applied a linear transformation proposed by Huang et al. (2006) to the full spectrum value of NDVI (−1.0–1.0) by setting the minimum value at 0.0 kPa and the range at 50.0 kPa. Finally, a 10-m digital elevation model (DEM) compiled from the stereo pairs of 1:5000 aerial photographs was used to calculate local slope angle and upslope contributing drainage area. The 10-m raster also became the basis for calculating the critical rainfall.

Table 2
Input soil parameters to the critical rainfall model

Lithological unit	n	ρ_s±SD	T±SD	φ±SD
Aoti formation	6	1.79±0.18	89.5±14.5	35.7±4.6
Tatungshan formation	5	1.82±0.25	61.1±13.8	33.2±5.2
Kanko formation	3	1.72±0.10	75.4±16.1	32.5±7.5

n: sample size; ρ_s: soil bulk density [g cm^{-3}]; T: transmissivity [m^2 day^{-1}]; φ: internal friction angle [°].

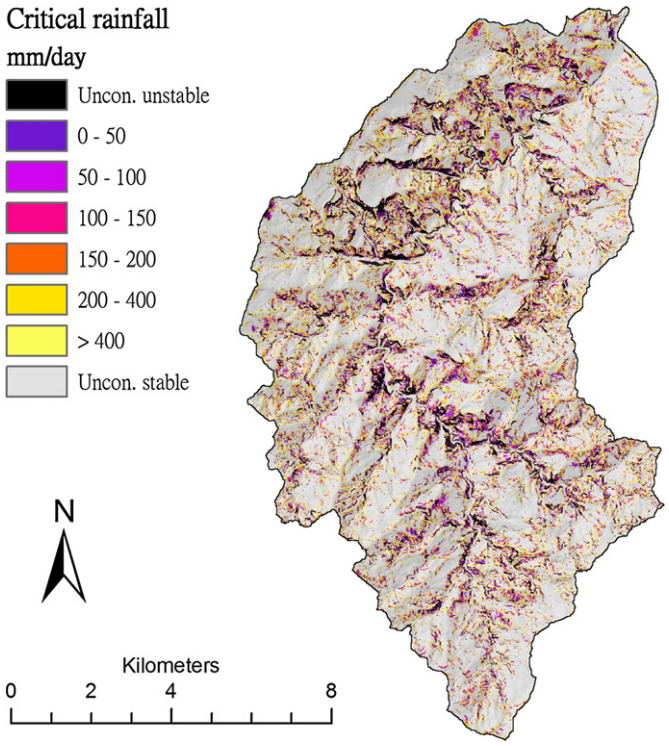

Fig. 3. Map of the critical rainfall for the Baichi watershed.

3.5. Logistic regression

Logistic regression uses a dependent variable y that is categorical (e.g., presence or absence) and explanatory variables x_i that are categorical, numeric, or both (Menard, 2002). Logistic regression has the following form:

$$\text{logit}(y) = a + b_1x_1 + b_2x_2 + b_3x_3 + \ldots + e \tag{5}$$

where a is a constant, b_i is the ith regression coefficient, and e is the error term. The logit of y is the natural logarithm of the odds:

$$\text{logit}(y) = \ln\left(\frac{p}{1-p}\right) \tag{6}$$

where p is the probability of the occurrence of y. To convert logit (y) back to the probability p, Eq. (6) can be rewritten as:

$$p = \frac{\exp(a + b_1x_1 + b_2x_2 + b_3x_3 + \ldots)}{1 + \exp(a + b_1x_1 + b_2x_2 + b_3x_3 + \ldots)} \tag{7}$$

A logit model is typically evaluated by the receiver operating characteristic (ROC) curve, which is based on the proportions of incidences correctly reported as positive (true positive) and incidences erroneously reported as positive (false positive). The area under the ROC curve (AUC) can measure the fitness of a model: the larger the area, the better the model. Additionally, Cox and Snell R^2 and Nagelkerke R^2 measure how well the explanatory variables can predict and explain the dependent variable (Menard, 2002). Cox and Snell R^2 cannot achieve a maximum of 1, whereas Nagelkerke R^2 stretches the R^2 value to range from 0 to 1.

In this study, the dependent variable y separated landslide (1) from non-landslide (0), and the explanatory variables were RID (x_1) and rainfall duration (x_2). The unit of analysis was a 10-m cell. For each of the 421 landslides triggered by Typhoon Aere, RID and rainfall duration were recorded at the cell corresponding to its centroid location. A random sample of 421 non-landslide cells was selected from conditionally stable and unstable areas of the critical rainfall model, and RID and rainfall duration were recorded for each cell.

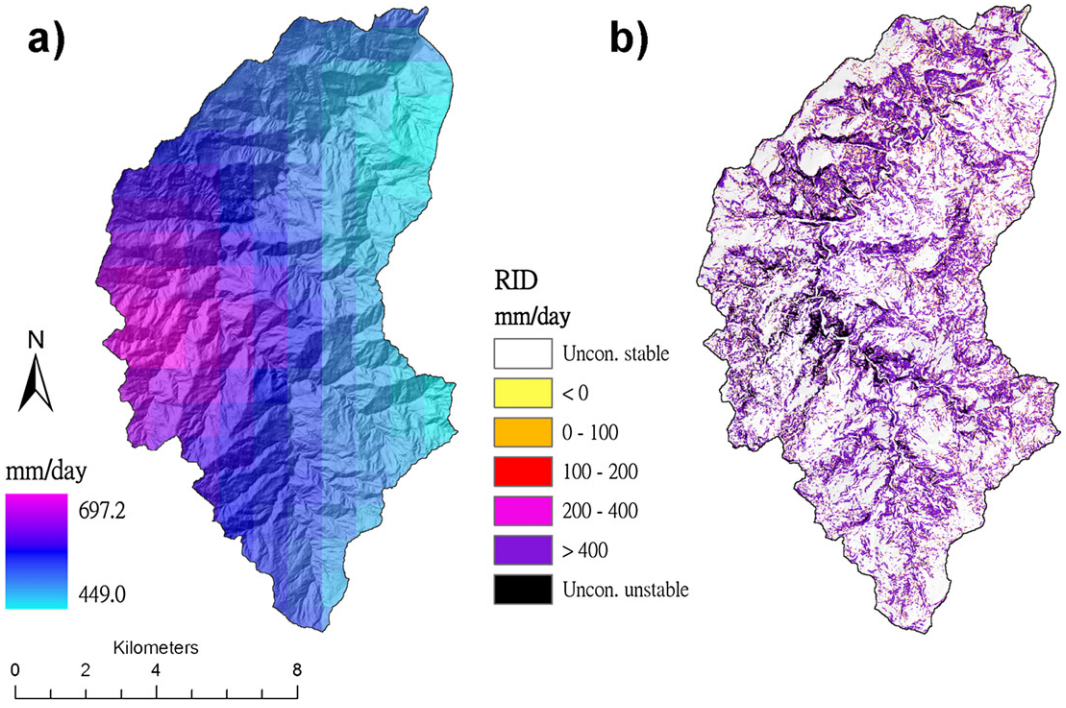

Fig. 4. Distributions of (a) estimated maximum 24-h rainfall intensity and (b) RID associated with Typhoon Aere.

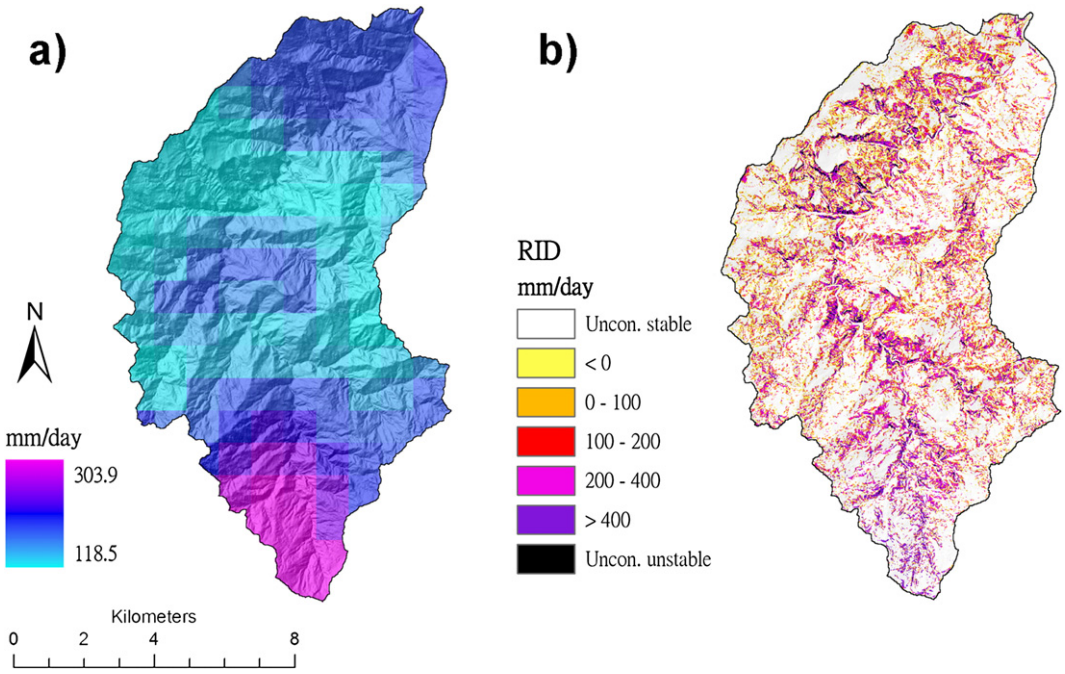

Fig. 5. Distributions of (a) estimated maximum 24-h rainfall intensity and (b) RID associated with Typhoon Haitang.

3.6. Assessment of model performance

To assess the accuracy of the model performance, this study used the modified success rate (MSR) defined as (Huang and Kao, 2006):

$$MSR = 0.5(SR_{number} \text{ for landslides}) + 0.5(SR_{cell} \text{ for stable areas}) \quad (8)$$

where SR_{number} is the rate of successfully predicted landslides [%] and SR_{cell} is the area proportion of successfully predicted stable areas [%]. By having two equally weighted components, MSR considers the predictability of both landslide sites and stable areas. For example, if a model successfully predicts 90% of landslides and only 50% of stable area cells, MSR of the model has a value of 0.70.

4. Results

4.1. Critical rainfall

Fig. 3 shows the distribution of critical rainfall ranges. Lower thresholds (i.e., higher potentials for slope failure) principally occupy steep slopes and large upstream contributing areas. In contrast, higher critical rainfall thresholds are present in ridges and gentle slopes.

4.2. Estimated 24-h rainfall intensity and RID

Fig. 4 shows the distributions of estimated maximum 24-h rainfall intensity (a) and RID (b) associated with Typhoon Aere. The rainfall intensity is highest in the west (>690 mm day^{-1}) and decreases gradually to the east (<450 mm day^{-1}). RID is high and positive where the critical rainfall threshold is low. Negative RID values are few and scattered. Fig. 5 shows the distributions of estimated maximum 24-h rainfall intensity (a) and RID (b) associated with Typhoon Haitang. The rainfall intensity is highest in the south (>300 mm day^{-1}), decreases toward the center, and then increases slightly to the north. The spatial pattern of RID is similar to that of Typhoon Aere except that the positive values are lower in magnitude. Also, there are many more negative values (i.e., estimated rainfall intensity<critical rainfall threshold).

Table 3
Logistic regression results

Variables	β	S.E.	Wald	df	Sig.	Exp(β)
RID	0.173	0.02	82.18	1	<0.01	1.80
Duration	0.584	0.16	13.36	1	<0.01	1.19
Constant	−38.59	9.33	17.10	1	<0.01	0.00

β represent the estimated regression coefficients for the explanatory variables, with the standard error (S.E.) given. The Wald statistic is the ratio of β to S.E. of the regression coefficient squared. *df* is the degree of freedom. The significance of each explanatory (Sig.) is given by the *p* value. Exp(β) is the predicted change in odds for a unit increase in the explanatory variable.

4.3. The integrated model

The integrated model is significant at the 1% level (AUC=0.79, Cox and Snell R^2=0.35, and Nagelkerke R^2=0.47). Both explanatory variables are also significant at the 1% level, with RID being more important than rainfall duration in explaining landslide occurrence (Table 3). Table 4 shows the model performance in terms of SR_{number}, SR_{cell}, and MSR. The integrated model has an MSR value of 84.0%, with both SR_{number} and SR_{cell} above 80.0%.

4.4. Model validation

Landslides triggered by Typhoon Haitang were used for validating the model derived from the landslide and rainfall data associated with Typhoon Aere. Using 0.5 as the threshold (i.e., landslide prediction is correct if p>0.5), the model has an MSR value of 87.4%, with both

Table 4
Performance of the integrated model in predicting landslides triggered by Typhoon Aere and Haitang

Event	Observation	Predictions		SR_{cell}	SR_{number}	MSR
		Stable areas	Landslides			
Aere	Stable areas	80.2	19.8	80.2	87.9	84.0
	Landslides	12.1	87.9			
Haitang	Stable areas	87.6	12.4	87.6	87.3	87.4
	Landslides	12.7	87.3			

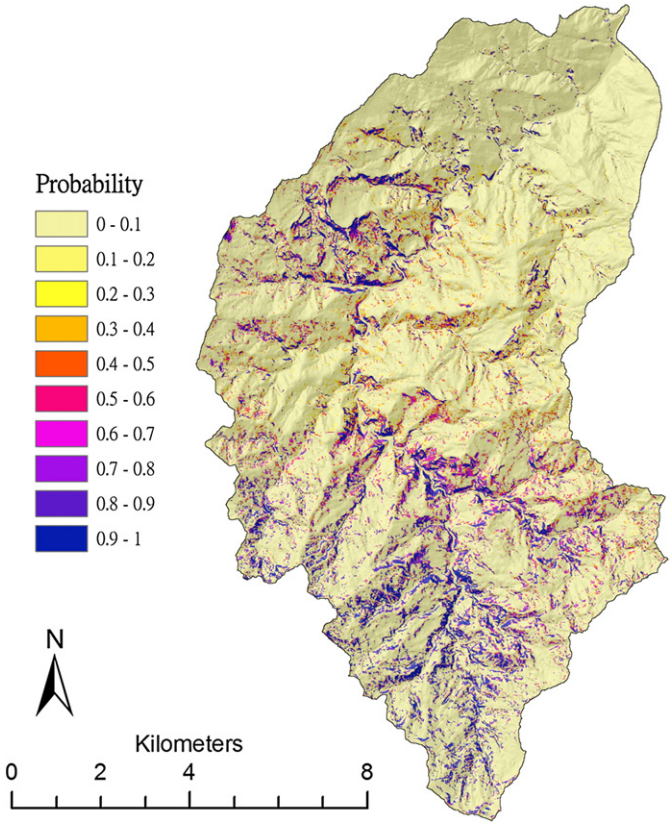

Fig. 6. Distribution of landslides triggered by Typhoon Haitang and calculated landslide probabilities from the integrated model.

SR_{number} and SR_{cell} above 87.0% (Table 4). Fig. 6 plots landslides triggered by Typhoon Haitang against calculated probabilities from the integrated model. Fig. 7 plots the distribution of landslides by probability. About 70% of landslides are located in the probability classes of 0.7 and above.

5. Discussion

5.1. Rainfall duration

The integrated model uses rainfall duration, a variable not considered by the critical rainfall model, for landslide prediction. To clarify the advantage of using rainfall duration, we compared the prediction results from the two models for landslides associated with Typhoon Haitang, which had lower rainfall intensity but longer duration than Typhoon Aere. The critical rainfall model has an MSR value of 75.4%, substantially lower than the integrated model's 87.4%. Of 87 landslides that could not be correctly predicted by the critical rainfall model, 54 (62%) were successfully predicted by the integrated model (Table 5). These landslide areas had a higher mean rainfall duration than areas where landslides were correctly predicted by the critical rainfall model ($p=0.02$), but their mean rainfall intensities were statistically the same ($p=0.32$) (Table 6). This result confirms the advantage of including rainfall duration in a landslide prediction model (Aleotti, 2004; Godt et al., 2006; Chang et al., 2008).

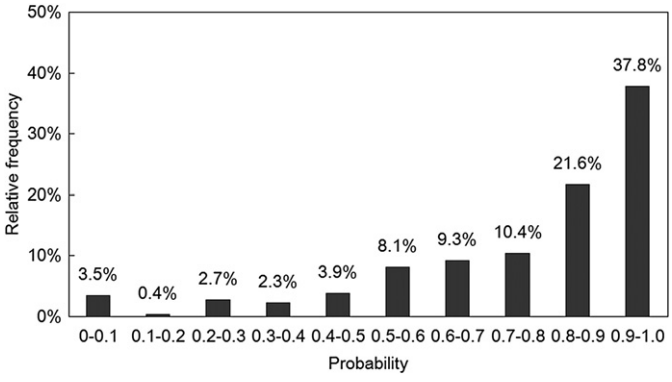

Fig. 7. Relative frequencies of landslides by calculated landslide probability.

Table 5
Comparison of the integrated model and the critical rainfall model (CRM) in predicting landslide occurrence

Integrate model	Predicted landslides	226	Predicted by CRM	172
			Unpredicted by CRM	54
	Unpredicted landslides	33	Predicted by CRM	0
			Unpredicted by CRM	33

5.2. RID

RID measures the rainfall intensity difference between radar rainfall estimate and the critical (minimum steady-state) rainfall, a rainfall rate calculated from local topographic and soil attributes. When used as an explanatory variable in the integrated model, RID complements the control of topographic and soil attributes by adding the triggering rainfall intensity into consideration. To illustrate the advantage of using RID, we compared the integrated model with a logit model based on maximum 24-h rainfall intensity and rainfall duration for predicting landslides triggered by Typhoon Aere. It should be noted that, due to the data sources, the logit model had a spatial resolution of 1 km whereas the integrated model 10 m. Table 7 shows that the integrated model has a higher MSR value than the logit model. For predicting stable areas (SR_{cell}), the logit model is only slightly better than random (54.2%). Without the aid of topographic and soil attributes, the logit model cannot separate stable areas from unstable areas.

5.3. The integrated model vs. the critical rainfall model

The integrated model is a statistical model that uses the prediction from the critical rainfall model to prepare one of the two explanatory variables. The integrated model does not explain how higher rainfall intensity can mechanically increase the potential of landslide occurrence. Nor does it explain the effect of rainfall intensity and rainfall duration on pore water pressure response to transient unsaturated flow. But, as the results of this study have demonstrated, the integrated model outperforms the critical rainfall model in predicting landslides. The integrated model is therefore a useful tool for watershed management. Moreover, given a pair of RID and rainfall duration, the integrated model can estimate the probability for landslide occurrence. In general, a probabilistic assessment is more helpful than a deterministic assessment for decision-making by watershed managers (Dai et al., 2002).

Table 6
t-tests of rainfall factors between landslides correctly predicted by the critical rainfall model (Case 1, $n=172$) and landslides not predicted by the critical rainfall model but predicted by the integrated model (Case 2, $n=54$)

Rainfall factor	Case	Mean	SD	*p*
RID (mm h^{-1})	1	6.07	1.34	0.322
	2	6.15	1.06	
Duration (h)	1	76.85	4.11	0.020
	2	75.68	3.43	

Table 7
Comparison of performance between the logit model and the integrated model

Typhoon event	Model comparison	SR_{number}	SR_{cell}	MSR
Aere	Logit model	90.4	54.2	72.3
	Integrated model	87.9	80.3	84.0

5.4. Application of the integrated model

The integrated model requires reliable estimates of rainfall distribution and detailed soil and topographic parameters for landslide prediction. Data availability and accuracy can be problematic for applications of the model. The accuracy of rainfall estimates from radar data can be complicated by such factors as miscalibrated radar, ground clutter, beam blockage, beam overshooting, non-uniform vertical profile of reflectivity, and uncertainty in the conversion of reflectivity to rainfall rate (Howard et al., 1997; Krajewski and Smith, 2002; Steiner and Smith, 2002). Different algorithms are also available for calibrating radar rainfall estimates with gauging station data (Wilson, 1970; Xin et al., 1997; Fulton et al., 1998; Hossain et al., 2004; Kalinga and Gan, 2006; Haberlandt, 2007). Users of radar data must choose an appropriate calibration method and conduct an accuracy assessment of radar rainfall estimate.

The accuracy of soil and topographic parameters in the critical rainfall model can also be influenced by a number of factors. Soil depth, hydraulic conductivity, and internal friction angle often exhibit considerable differences between suitable values used in model calculation and measured values from field sampling. For example, both Onda et al. (2003) and Morrissey et al. (2004) used a calibrated value of hydraulic conductivity, an order of magnitude greater than that obtained from laboratory measurements. This kind of discrepancy may be unavoidable because it is caused by the spatial and temporal variability of the parameters. Soil depth and permeability may also change from one landsliding episode to another, especially in mountainous watersheds with frequent landslide occurrences. In turn, these changes can affect the prediction capability of a model based on the constant values of a few soil and vegetation parameters.

The scaling issue is another concern for model applications. In this study, the spatial resolution is 1 km for radar rainfall estimate and 10 m for the critical rainfall. Although the incompatibility of scales or resolutions is common in landslide studies (e.g., 1:5000-scale soil layer versus 1:50,000-scale geology layer), it can create problems in interpreting and applying results. For example, the incompatibility makes it difficult for this study to directly assess the relative importance of rainfall factors versus topographic and soil parameters in causing landslides.

6. Conclusion

This study has presented a novel approach that incorporates a deterministic slope stability model, a logit model, and radar-derived rainfall data into landslide prediction. Based on the results of model performance, the integrated model appears to be better than 'traditional' models for predicting landslide occurrence. Compared with the critical rainfall model, the new model has the advantage of including rainfall duration in addition to rainfall intensity for improving the predictability of landslide occurrence. Compared with the logit model based on rainfall variables, the integrated model has the advantage of bringing topographic and soil properties into logistic regression analysis through the rainfall intensity difference variable. The integrated model is expected to improve prediction of future landslides in the study area, a mountainous watershed in northern Taiwan. It can also be applied to other areas if adequate rainfall data and topographic and soil measurements are available.

Acknowledgments

This work was supported by grants from Taiwan's National Science Council (96-2415-H-424-005-MY2, 97-2923-H-424-001-MY2). We thank an anonymous referee and the editor for their helpful comments.

References

Aleotti, P., 2004. A warning system for rainfall-induced shallow failures. Engineering Geology 73, 247–265.
Aleotti, P., Chowdhury, R., 1999. Landslide hazard assessment: summary review and new perspectives. Bulletin of Engineering Geology and the Environment 58, 21–44.
Au, S.W.C., 1993. Rainfall and slope failure in Hong Kong. Engineering Geology 36, 141–147.
Ayalew, L., Yamagishi, H., 2005. The application of GIS-based logistic regression for landslide susceptibility in the Kakuda-Yahiko Mountains, Central Japan. Geomorphology 65, 15–31.
Baum, R.L., Coe, J.A., Godt, J.W., Harp, E.L., Reid, M.E., Savage, W.Z., Schulz, W.H., Brien, D.L., Chleborad, A.F., McKenna, J.P., Michael, J.A., 2005. Regional landslide-hazard assessment for Seattle, Washington, USA. Landslides 2, 266–279.
Borga, M., Dalla Fontana, G., Gregoretti, C., Marchi, L., 2002. Assessment of shallow landsliding by using a physically based model of hillslope stability. Hydrological Processes 16, 2833–2851.
Caine, N., 1980. The rainfall intensity-duration control of shallow landslides and debris flows. Geografiska Annaler 62A, 23–27.
Campbell, R.H., 1975. Soil slips, debris flows, and rainstorms in the Santa Monica Mountains and vicinity, southern California. USGS Professional Paper 851. US Geological Survey, Reston, VA.
Can, T., Nefeslioglu, H.A., Gokceoglu, C., Sonmez, H., Duman, T.Y., 2005. Susceptibility assessments of shallow earthflows triggered by heavy rainfall at three catchments by logistic regression analyses. Geomorphology 72, 250–271.
Cannon, S.H., Ellen, S., 1985. Rainfall conditions for abundant debris avalanches in the San Francisco Bay region, California. California Geology 38, 267–272.
Carrara, A., Crosta, G., Frattini, P., 2008. Comparing models of debris-flow susceptibility in the alpine environment. Geomorphology 94, 353–378.
Casadei, M., Dietrich, W.E., Miller, N.L., 2003. Testing a model for predicting the timing and location of shallow landslide initiation in soil-mantled landscapes. Earth Surface Processes and Landforms 28, 925–950.
Chang, K., Chiang, S., Hsu, M., 2007. Modeling typhoon- and earthquake-induced landslides in a mountainous watershed using logistic regression. Geomorphology 89, 335–347.
Chang, K., Chiang, S., Feng, L., 2008. Analysing the relationship between typhoon-triggered landslides and critical rainfall conditions. Earth Surface Processes and Landforms 33, 1261–1271.
Chen, C., Chen, T., Yu, F., Yu, W., Tseng, C., 2005. Rainfall duration and debris-flow initiated studies for real-time monitoring. Environmental Geology 47, 715–724.
Chen, C., Lin, L., Yu, F., Lee, C., Tseng, C., Wang, A., Cheung, K., 2007. Improving debris flow monitoring in Taiwan by using high-resolution rainfall products from QPESUMS. Natural Hazards 40, 447–461.
Claessens, L., Schoorl, J.M., Veldkamp, A., 2007. Modelling the location of shallow landslides and their effects on landscape dynamics in large watersheds: an application for Northern New Zealand. Geomorphology 87, 16–27.
Creutin, J.D., Borga, M., 2003. Radar hydrology modifies the monitoring of flash flood hazard. Hydrological Processes 17, 1453–1456.
Crozier, M.J., 1999. Prediction of rainfall-triggered landslides: a test of the antecedent water status model. Earth Surface Processes and Landforms 24, 825–833.
Dai, F.C., Lee, C.F., 2003. A spatiotemporal probabilistic modelling of storm-induced shallow landsliding using aerial photographs and logistic regression. Earth Surface Processes and Landforms 28, 257–545.
Dai, F.C., Lee, C.F., Ngai, Y.Y., 2002. Landslide risk assessment and management and management — an overview. Engineering Geology 64, 65–87.
Finlay, P.J., Fell, R., Maguire, P.K., 1997. The relationship between the probability of landslide occurrence and rainfall. Canadian Geotechnical Journal 34, 811–824.
Fulton, R.A., Breidenbach, J.P., Seo, D., Miller, D.A., 1998. The WSR-88D rainfall algorithm. Weather Forecast 13, 377–395.
Glade, T., Crozier, M.J., Smith, P., 2000. Applying probability determination to refine landslide-triggering rainfall thresholds using an empirical "Antecedent Daily Rainfall Model". Pure and Applied Geophysics 157, 1059–1079.
Godt, J.W., Baum, R.L., Chleborad, A.F., 2006. Rainfall characteristics for shallow landsliding in Seattle, Washington, USA. Earth Surface Processes and Landforms 31, 97–110.
Gorsevski, P.V., Gessler, P.E., Bill, J., Elliot, W.J., Foltz, R.B., 2006. Spatial and temporally distributed modeling of landslide susceptibility. Geomorphology 80, 178–198.
Guzzetti, F., Carrara, A., Cardinali, M., Reichenbach, P., 1999. Landslide hazard evaluation: a review of current techniques and their application in a multi-scale study, Central Italy. Geomorphology 31, 181–216.
Guzzetti, F., Cardinali, M., Reichenbach, P., Cipolla, F., Sebastiani, C., Galli, M., Salvati, P., 2004. Landslides triggered by the 23 November 2000 rainfall event in the Imperia Province, Western Liguria, Italy. Engineering Geology 73, 229–245.
Haberlandt, U., 2007. Geostatistical interpolation of hourly precipitation from rain gauges and radar for a large-scale extreme rainfall event. Journal of Hydrology 332, 144–157.

Hossain, F., Anagnostou, E.N., Dinku, T., Borga, M., 2004. Hydrological Processes 18, 3277–3291.
Hovius, N., Stark, C.P., Allen, P.A., 1997. Sediment flux from a mountain belt derived by landslide mapping. Geology 25, 231–234.
Howard, K.W., Gourley, J.J., Maddox, R.A., 1997. Uncertainties in WSR-88D measurements and their impacts on monitoring life cycles. Weather Forecast 12, 166–174.
Huang, J.C., Kao, S.J., 2006. Optimal estimator for measuring landslide model efficiency. Hydrology and Earth System Sciences 10, 957–965.
Huang, J.C., Kao, S.J., Hsu, M.L., Lin, J.C., 2006. Stochastic procedure to extract and to integrate landslide susceptibility maps: and example of mountainous watershed in Taiwan. Natural Hazards and Earth System Sciences 6, 803–815.
Ibsen, M.-L., Casagli, N., 2004. Rainfall patterns and related landslide incidence in the Porretta-Vergato region, Italy. Landslides 1, 143–150.
Kalinga, O.A., Gan, T.Y., 2006. Semi-distributed modelling of basin hydrology with radar and gauged precipitation. Hydrological Processes 20, 3725–3746.
Krajewski, W.F., Smith, J.A., 2002. Radar hydrology: rainfall estimation. Advance Water Research 25, 1387–1394.
Larsen, M.C., Simon, A., 1993. A rainfall intensity–duration threshold for landslides in a humid–tropical environment. Geografiska Annaler Series A 75, 13–23.
Menard, S., 2002. Applied Logistic Regression Analysis, 2nd ed. Sage, Thousand Oaks, CA.
Montgomery, D.R., Dietrich, W.E., 1994. A physically based model for topographic control on shallow landsliding. Water Resources Research 30, 1153–1171.
Montgomery, D.R., Sullivan, K., Greenberg, H.M., 2002. Regional test of a model for shallow landsliding. Hydrological Processes 12, 943–955.
Morrissey, M.M., Wieczorek, G.F., Morgan, B.A., 2004. Transient hazard model using radar data for predicting debris flows in Madison County, Virginia. Environmental & Engineering Geoscience 10, 285–296.
Ohlmacher, G.C., Davis, J.C., 2003. Using multiple logistic regression and GIS technology to predict landslide hazard in northeast Kansas, USA. Engineering Geology 69, 331–343.
Onda, Y., Mizuyama, T., Kato, Y., 2003. Judging the time of rainfall-triggered debris flows by monitoring runoff. 3rd International Conference on Debris-Flow Hazard Mitigation, Davos, Switzerland, pp. 147–153.
Pack, R.T., Tarboten, D.G., Goodwin, C.N., 1998. GIS-based landslide susceptibility mapping with SINMAP. Proceedings: 34th Symposium on Engineering Geology and Geotechnical Engineering, April 28–30, Logan, Utah, pp. 219–231.
Steiner, M., Smith, J.A., 2002. Use of three-dimensional reflectivity structure for automated detection and removal of nonprecipitating echoes in radar data. Journal of Atmospheric and Oceanic Technology 19, 673–686.
Wilson, J.W., 1970. Integration of radar and raingage data for improved rainfall measurement. Journal of Applied Meteorology 9, 489–497.
Wu, W., Sidle, R.C., 1995. A distributed slope stability model for steep forested basins. Water Resources Research 31, 2098–2110.
Wu, C.C., Kuo, Y.H., 1999. Typhoons affecting Taiwan: current understanding and future challenges. American Meteorological Society Bulletin 80, 67–80.
Xin, L., Reuter, G., Larochelle, B., 1997. Reflectivity–rain rate relationships for convective rainshowers in Edmonton. Atmosphere-Ocean 35, 513–521.
Yesilnacar, E., Topal, T., 2005. Landslide susceptibility mapping: a comparison of logistic regression and neural networks methods in a medium scale study, Hendek region (Turkey). Engineering Geology 79, 251–266.